

Effect of Constituent Materials on Composite Performance: Exploring Design Strategies via Machine Learning

Chun-Teh Chen and Grace X. Gu*

Nature assembles a range of biological composites with remarkable mechanical properties despite being composed of relatively weak polymeric and ceramic components. However, the architectures of biomaterials cannot be considered as optimal designs for engineering applications since biomaterials are constantly evolving for multiple functions beyond carrying external loading. Here, it is aimed to develop an intelligent approach to design superior composites from scratch—starting from constituent materials. A systematic computational investigation of the effect of constituent materials (assumed to be perfectly brittle) on the behavior of composites using an integrated approach combining finite element method, molecular dynamics, and machine learning (ML) is reported. It is demonstrated that instead of using brute-force methods, machine learning is a much more efficient approach and can generate optimal designs with similar performance to those obtained from an exhaustive search. Furthermore, it is shown that the toughening and strengthening mechanism observed in composites at the continuum-scale by combining stiff and soft constituents is valid for nanomaterials as well. Results show that high-performing designs of graphene nanocomposites can be generated using our ML approach. This novel ML-based design framework can be applied to other material systems to study a variety of structure–property relationships over several length-scales.

materials (base materials) in a particular predetermined architecture. The base materials often have very distinctive properties and can work together to create composites with properties different from their constituents. From the engineering point of view, the base materials should be placed in an optimal architecture to achieve the highest performance for a given design objective. However, traditional manufacturing methods have limited composite architectures to mostly laminate structures, with stacked layers consisting of fibers in a matrix material. Thus, the full potential of composites, with their vast design space, is difficult to be realized. In recent years, with advances in additive manufacturing, it is now possible to create complex composite architectures that consist of internal voids, multiple materials, and irregular shapes.^[3] Facilitating novel fabrication techniques enables higher resolution and more precise control compared to traditional manufacturing methods.^[4] Specifically, advanced manufacturing leads to the possibility of biomimicry, where many natural materials (i.e., nacre and bone) are comprised of complex architectures over several length-scales.

1. Introduction

Creating new structural materials with superior mechanical properties while still being economically efficient is one of the ultimate goals of modern engineering applications.^[1] Composites are widely used in the design of structural materials in order to satisfy specific property requirements.^[2] The essential trait of composites lies in the ability to combine two or more constituent

Nature hosts an elegant and plentiful array of adequate solutions for achieving superior mechanical properties under material composition constraints. Studying the architectures of biomaterials, we are able to learn various design strategies as to how organisms evolve to survive in their environments and apply that knowledge to create new engineering materials. This approach is often referred to as biomimicry and pursuant designs are termed bioinspired.^[5,6] Nevertheless, the architectures of biomaterials cannot be considered as optimal designs, at least in terms of mechanical properties. This is due to the fact that organisms are evolving biomaterials for multiple functions, such as for catching prey or transporting nutrients, not only for carrying external loading. Additionally, organisms are limited to the material constituents available in their surroundings and those that can be produced via biosynthesis. As optimal designs of composites highly depend on the properties of base materials, creating new composites by just mimicking the architectures of biomaterials but using different base materials is not an ideal approach. While biomaterials are important sources of inspiration, we should view them more like a flexible template rather than a rigid recipe. Thus, it is crucial to develop an intelligent approach to design composites from scratch. Various optimization

C.-T. Chen
Department of Materials Science and Engineering
University of California
Berkeley, CA 94720, USA

G. X. Gu
Department of Mechanical Engineering
University of California
Berkeley, CA 94720, USA
E-mail: ggu@berkeley.edu

 The ORCID identification number(s) for the author(s) of this article can be found under <https://doi.org/10.1002/adts.201900056>

DOI: 10.1002/adts.201900056

methods, such as greedy algorithms and gradient-based algorithms, are widely applied to design composites and some other design problems for different objectives.^[7] However, as composite design problems are usually nonconvex, the optimal solutions obtained from those optimization methods often depend on the initial geometry adopted in the optimization process. Consequently, the solutions not only vary from one initial geometry to another but also, in some cases, can be stuck in poor local minima (or critical points). On the other hand, machine learning (ML), a data-driven approach, is a promising alternative method to design composites.^[8–10] Recent rapid advances in ML techniques showed various successful applications in the field of computational mechanics. We have demonstrated that ML techniques can accelerate the composite design process by learning the structure–property relationships from training data.^[9,10] Hanakata et al. reported how ML techniques can be applied to the design of kirigami-inspired stretchable materials.^[11]

Three major factors that affect the mechanical properties of composites are: i) the properties of base materials; ii) the topology (architecture) of how base materials are placed spatially; iii) the volume fraction of base materials. In this work, all these three factors will be explored to study their effects on composite performance under *Mode I* fracture. Specifically, we aim to understand how the modulus, toughness, and volume fraction of base materials (assumed to be perfectly brittle) affect the effective toughness, strength, and stiffness of composites, as well as how the optimal designs vary when different base materials are chosen for creating composites. Results in this work provide guidelines for choosing base materials to create composites with superior mechanical properties. Note that searching for the optimal designs of composites is extremely challenging due to the astronomical number of possible material and geometrical combinations. Equipped with these tools on how to choose base materials to create composites with desired properties, the selection of base materials is no longer a design variable. Thus, the design space can be significantly reduced following the design guidelines formulated in this work. Moreover, we demonstrate a computational design approach combining machine learning and finite element method (FEM) for creating tougher and stronger composites. With this, we aim to develop highly accurate and efficient ML models for composite design problems. Finally, we explain the physics of the toughening and strengthening mechanism observed in composites. Note that some toughening mechanisms have been shown to be effective at several different length-scales. For instance, the toughening mechanism of nacre comes from its “brick-and-mortar” structure, in which stiff aragonite tablets (5–15 μm in diameter) are glued together with soft biopolymer. This “brick-and-mortar” structure has been applied to design composites (in the scale of centimeters) and graphene–oxide nanocomposites (in the scale of nanometers).^[5] Here, we are interested in whether the toughening and strengthening mechanism observed in composites (continuum-scale) due to the geometrical effect of combining stiff and soft materials is also valid for nanomaterials (nanoscale). In this case study, we use graphene and hydrogenated graphene as base materials to create a graphene nanocomposite with the topology designed by machine learning. Molecular dynamic (MD) simulations are performed to investigate the mechanical

responses of the graphene nanocomposite and its base materials. The MD results are compared with the ML predictions.

2. Results and Discussion

2.1. Effect of Base Material Modulus Ratio

In this work, we consider composites made up of perfectly brittle linear elastic materials, in which materials do not exhibit yielding (plastic deformation) before failure. The toughness of such material can be quantified as the amount of elastic energy per unit volume that the material can absorb prior to failure, which can be written as:

$$T = \int_0^{\varepsilon_f} \sigma d\varepsilon = \frac{E\varepsilon_f^2}{2} = \frac{\sigma_f^2}{2E} \quad (1)$$

where T is the toughness, E is the Young's modulus, ε_f is the failure strain, and σ_f is the failure stress (material strength). There are several ways to describe the mechanical behavior (stress–strain curve) of a material undergoing catastrophic failure by using a combination of these material properties (i.e., T , E , ε_f , and σ_f). Equation (1) shows that any two of these material properties can sufficiently define the mechanical behavior of a material. In this work, to study the effect of base materials on composite performance, the modulus E and toughness T of base materials are used as the two design variables. We start the investigation with a simple composite system, an 8 by 8 composite system made up of two base materials, in which one of them is a stiff material and the other is a soft material. The details of this composite system are shown in Figure S1, Supporting Information and described in the Experimental Section. The number of possible combinations in this composite system is 2^{32} (4 294 967 296) as geometrical symmetry is assumed. A brute-force search combined with finite element analysis is performed to calculate the performance (toughness, strength, and stiffness) of all possible combinations under *Mode I* fracture.

In this composite system, the modulus ratio of base materials is set to 10 and the toughness ratio is set to 1. The modulus ratio is defined as the modulus of the stiff material divided by that of the soft material; the toughness ratio is defined as the toughness of the stiff material divided by that of the soft material. A toughness ratio of 1 means that the stiff and soft materials have the same toughness. Thus, we can eliminate the effect of using base materials with different toughness and only focus on the geometrical effect of combining stiff and soft materials on composite performance. After the brute-force search, the optimal designs for high toughness with different volume fractions are identified and shown in Figure 1. The volume fraction is defined as the number of soft elements divided by the total number of elements. The volume fraction of 0% represents a completely stiff matrix; the volume fraction of 100% represents a completely soft matrix. Note that this volume fraction definition is different from that commonly used for fiber-reinforced composites, in which the volume fraction is usually defined as the fraction of stiff materials (i.e., fibers).

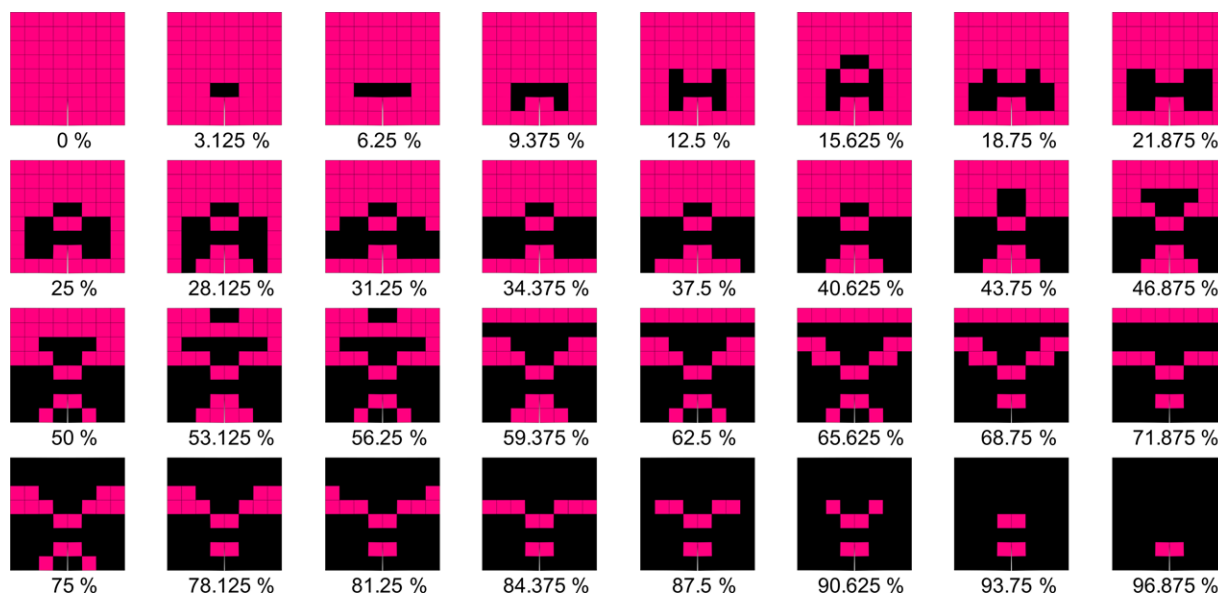


Figure 1. Optimal designs for high toughness, using base materials with the modulus ratio of 10 and toughness ratio of 1, for the 8 by 8 composite system. The results are obtained by the brute-force search for different volume fractions. The stiff elements are shown in pink and the soft elements are shown in black. The number below each optimal design is the volume fraction of the design.

The optimal designs for other objectives, including low toughness, high strength, low strength, high stiffness, and low stiffness, with different volume fractions are shown in Figures S2–S6, Supporting Information, respectively. With these optimal designs identified in this work, we can benefit from learning design strategies to achieve different objectives. For instance, it can be observed in Figure 1 that a common design strategy to achieve high toughness is to use the soft material for the crack-tip elements and the stiff material for the elements above and below the crack-tip elements (Figure S7, Supporting Information). The physical explanation of this design strategy is as follows: From Equation (1), it can be calculated that the failure strain of the soft material is considerably larger than that of the stiff material ($\epsilon_{f, \text{soft}}/\epsilon_{f, \text{stiff}} = 3.16$) in this composite system. Thus, using the soft material for the crack-tip elements helps postpone crack propagation. Additionally, using stiff materials for the elements above and below the crack-tip elements reduces the strain (ϵ_{xx}) of the crack-tip elements, thus increasing the toughness of the composites. It is discovered that this design strategy not only applies to this specific composite system. When the toughness of the base materials is the same, this design strategy applies to all composite systems made up of stiff and soft materials with different modulus ratios. More discussions on the effect of adding the soft material on composite toughness can be found in the Supporting Information.

To study the effect of the base material modulus ratio ($E_{\text{stiff}}/E_{\text{soft}}$) on composite performance, three composite systems with various modulus ratios (10, 5, and 2) are considered. The mechanical properties of these composite systems are shown in Figure 2. Different modulus ratios are achieved by varying the modulus of the soft material while keeping the modulus of the stiff material the same. Moreover, the toughness ratio is fixed to 1 in these composite systems. The toughness values shown in

Figure 2 are normalized by the toughness of the composite made up of all stiff material. The same normalization method is applied to the strength and stiffness values as well. The optimal designs for high toughness using base materials with the modulus ratios of 10, 5, and 2 are shown in Figure 1; Figures S8 and S9, Supporting Information, respectively. Although the optimal designs are slightly different when using base materials with different modulus ratios, it can be observed that the common design strategy proposed above applies to all these three composite systems. Comparing the toughness values of these three composite systems, the mean and maximum toughness (Figure 2a,b) increases as the modulus ratio increases. This is due to the fact that using the soft material with a lower modulus (higher modulus ratio) causes a larger influence (geometrical effect) on composite performance. Thus, higher maximum toughness (Figure 2b) and lower minimum toughness (Figure 2c) can be observed in the composite system with a higher modulus ratio. As the improvement on the maximum toughness (Figure 2b) is much more significant than the decrement on the minimum toughness (Figure 2c), the mean toughness (Figure 2a) increases as the modulus ratio increases. However, the mean strength (Figure 2d) does not always increase as the modulus ratio increases. From Equation (1), it can be calculated that the strength of the soft material decreases as the modulus ratio increases. Consequently, when the volume fraction is high (more soft material is added), the mean strength (Figure 2d) of the composite systems decreases as the modulus ratio increases. Higher maximum strength (Figure 2e) and lower minimum strength (Figure 2f) can also be observed in the composite system with a higher modulus ratio. Finally, using the soft material with a lower modulus (higher modulus ratio) reduces the stiffness (mean, maximum, and minimum) of the composite systems (Figure 2g–i). Thus, the stiffness of the composite systems decreases as the volume

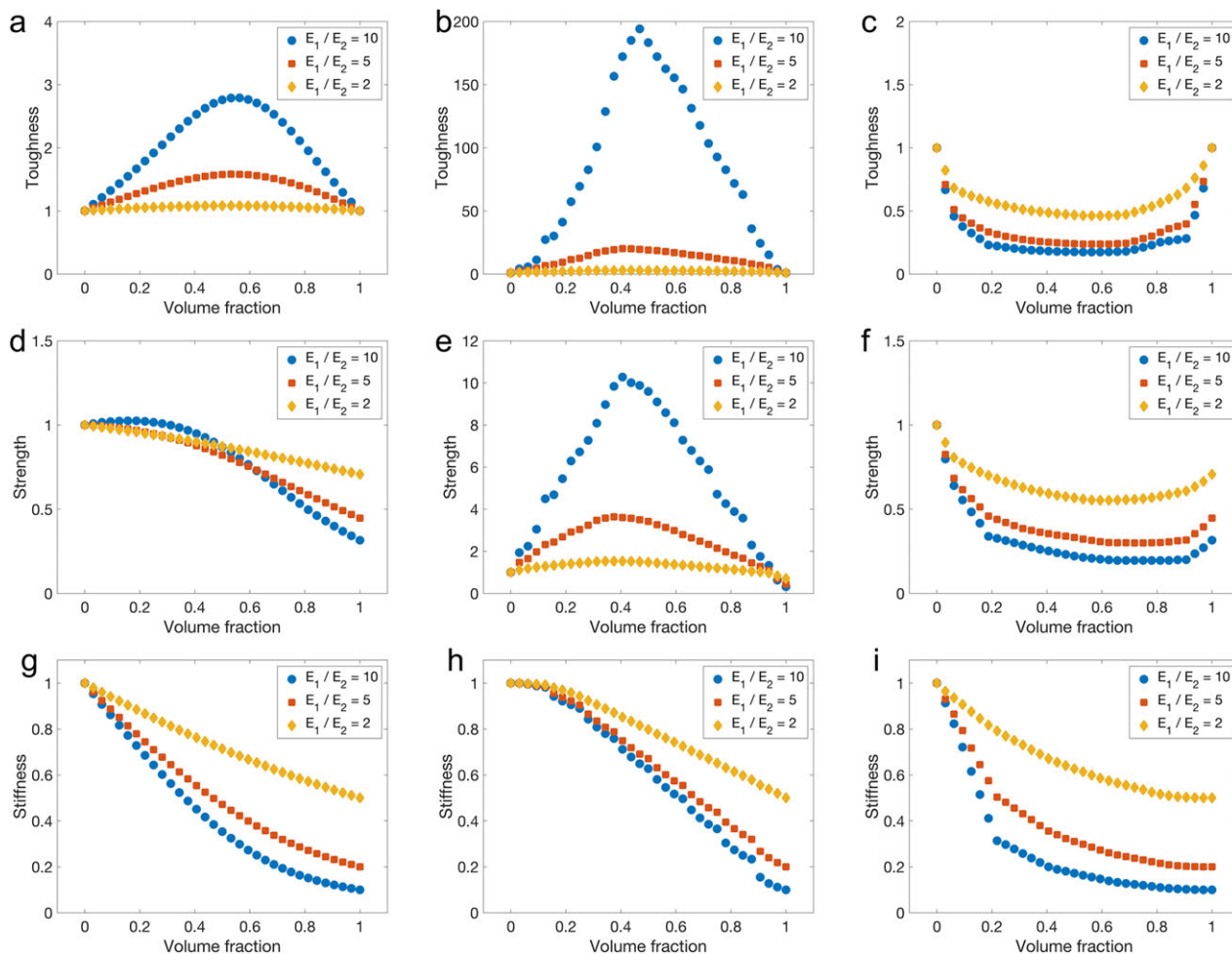


Figure 2. Effect of the base material modulus ratio on composite performance with different volume fractions. a–c) show the effect on the mean, maximum, and minimum toughness of the composites, respectively. d–f) show the effect on the mean, maximum, and minimum strength of the composites, respectively. g–i) show the effect on the mean, maximum, and minimum stiffness of the composites, respectively. The results are obtained by the brute-force search for the 8 by 8 composite systems with various modulus ratios, in which the toughness ratios are fixed to 1.

fraction increases (more soft material is added). The optimal volume fraction for high stiffness is 0% (no soft material is added), as expected.

2.2. Effect of Base Material Toughness Ratio

To study the effect of the base material toughness ratio ($T_{\text{stiff}}/T_{\text{soft}}$) on composite performance, three composite systems with various toughness ratios (1, 2, and 5) are considered. The mechanical properties of these composite systems are shown in **Figure 3**. Different toughness ratios are achieved by varying the toughness of the soft material while keeping the toughness of the stiff material the same. Moreover, the modulus ratio is fixed to 10 in these composite systems. In **Figure 3**, the toughness, strength, and stiffness values are normalized using the same normalization method applied to the results shown in **Figure 2**. To have a better comparison, the first composite system shown in **Figure 3**, with the toughness ratio of 1 and modulus ratio of 10, is the same as the first composite system shown in **Figure 2**. The optimal de-

signs for high toughness using base materials with the toughness ratios of 1, 2, and 5 are shown in **Figure 1**; **Figures S10 and S11**, Supporting Information, respectively. Comparing the toughness values of these three composite systems, the toughness (mean, maximum, and minimum) decreases as the toughness ratio increases (**Figure 3a–c**). This is due to the fact that using the soft material with a lower toughness (higher toughness ratio) reduces the overall toughness of the composite systems. However, the geometrical effect of combining stiff and soft materials can still make some composite designs tougher than a completely stiff matrix, even using the soft material with a lower toughness. Consequently, an improvement on the mean and maximum toughness can be observed when the volume fraction is not too high (**Figure 3a,b**).

From **Equation (1)**, it can be calculated that the strength of the soft material decreases as the toughness ratio increases. Thus, the strength (mean, maximum, and minimum) of the composite system decreases as the toughness ratio increases (**Figure 3d–f**). For the composite systems with a high toughness ratio (2 and 5), the mean strength decreases as the volume

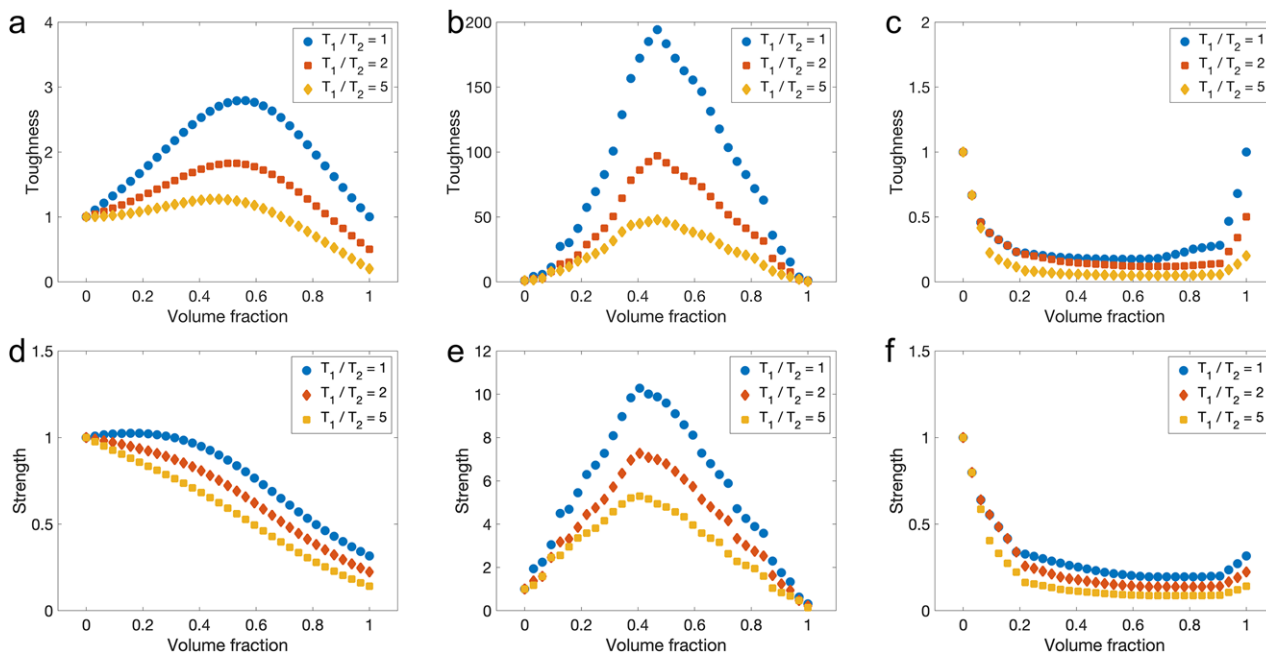


Figure 3. Effect of the base material toughness ratio on composite performance with different volume fractions. a–c) show the effect on the mean, maximum, and minimum toughness of the composites, respectively. d–f) show the effect on the mean, maximum, and minimum strength of the composites, respectively. The results are obtained by the brute-force search for the 8 by 8 composite systems with various toughness ratios, in which the modulus ratios are fixed to 10. The effect on the stiffness of the composites is not shown since changing only the toughness ratio of base materials does not affect the stiffness of the composites.

fraction increases (Figure 3d). Note that even using the soft material with a low toughness (low strength as well), the geometrical effect of combining stiff and soft materials can still make some composite designs stronger than a completely stiff matrix. Thus, an improvement in the maximum strength can be observed when the volume fraction is not too high (Figure 3e). The stiffness of the composite systems does not vary with the toughness ratio since the modulus ratio of the base materials is fixed. Thus, the effect of the toughness ratio of base materials on the stiffness of composites is not shown in Figure 3.

2.3. Performances of Various Machine Learning Models

In previous sections, we investigate composites at the continuum-scale and search for the optimal designs based on the properties of base materials. Here, we aim to understand whether the optimal designs identified at the continuum-scale can be transferred directly to a smaller length-scale composite system. We create a graphene nanocomposite system in which graphene and graphane (hydrogenated graphene) are chosen as the base materials. The design objective is to create a tougher and stronger graphene nanocomposite. We use the brute-force search in previous sections to study the effect of modulus and toughness ratios of base materials on composite performance, as well as to identify the optimal designs for various objectives. However, brute-force methods are very computationally expensive. For instance, to search for the optimal designs of an 8 by 8 composite system requires running 2^{32} (4 294 967 296) FEM simulations. For a larger composite system, using brute-force

methods to search for the optimal designs is computationally intractable. As demonstrated in our previous work,^[9,10] ML techniques can be applied to generate high-performing designs of composites by learning the structure–property relationships from a small amount of training data. Here, we extend our previous work to investigate the performance of different ML models for the graphene nanocomposite design problem. Three ML models including the linear model, nonlinear model, and convolutional neural network (CNN) model are investigated. The details of these ML models are described in the Experimental Section. To evaluate the performance of these ML models, we start with an 8 by 8 composite system. The modulus and toughness ratios of graphene and graphane (base materials) are set to 2 to mimic their actual material properties (to be discussed in the next section). The volume fraction is set to 50%, which gives the largest design space with around 600 million possible combinations. 800 000 training samples are used to train these ML models and 200 000 testing samples are used to evaluate their accuracy. After the training process (see the Experimental Section for details), these ML models are applied to predict the toughness of composites without running FEM simulations.

Comparisons of ML predictions and FEM results are shown in Figure 4. The loss in these ML models during the training process is shown in Figure S12, Supporting Information. Among these ML models, the linear model provides the lowest accuracy (highest error) with the mean squared error (MSE) of 0.04 for both training and testing data (Figure 4a). Additionally, the linear model performs much worse on the highly ranked samples (Figure 4b). The nonlinear model provides better accuracy with the MSE of 0.01 for both training and testing data

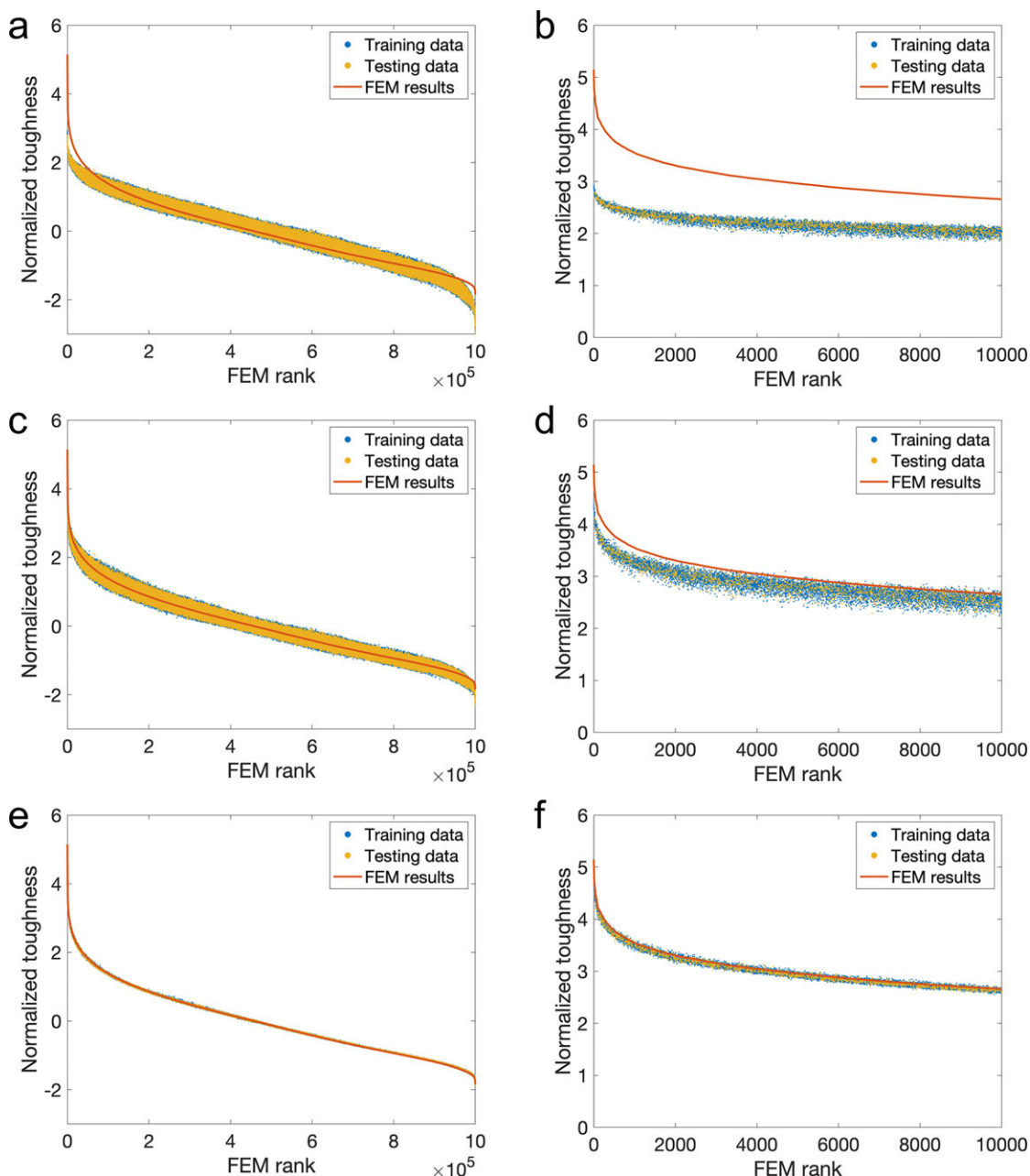


Figure 4. Comparisons of ML predictions and FEM results for toughness. The results in a) and b) are obtained by the linear model. The MSE in the linear model is 0.04 for both training and testing data. The results in c) and d) are obtained by the nonlinear model. The MSE in the nonlinear model is 0.01 for both training and testing data. The results in e) and f) are obtained by the CNN model. The MSE in the CNN model is 0.0002 for both training and testing data. (b), (d), and (f) are the zoomed-in results (top 10 000 FEM rank) of (a), (c), and (e), respectively. The 8 by 8 composite system with the volume fraction of 50%, in which the modulus and toughness ratios are set to 2, is used for the comparison. The number of possible combinations in this composite system is around 600 million. 800 000 training samples are used to train the ML models and 200 000 testing samples are used to evaluate their accuracy.

(Figure 4c). The performance of the nonlinear model on the highly ranked samples (Figure 4d) is also better than that of the linear model (Figure 4b) due to the additional nonlinear term in the hypothesis. Finally, the CNN model provides the highest accuracy with the MSE of 0.0002 for both training and testing data (Figure 4e). The performance of the CNN model on the highly ranked samples (Figure 4f) is also the best among these ML mod-

els since the CNN model has a much higher learning capacity (model complexity) than the other two ML models. However, to generate the optimal designs of composites, a searching process, such as sampling, screening, or optimization, is required when using the CNN model (or other complex ML models) for the composite design problem. As demonstrated in our previous work,^[10] where we used a CNN model together with a self-learning

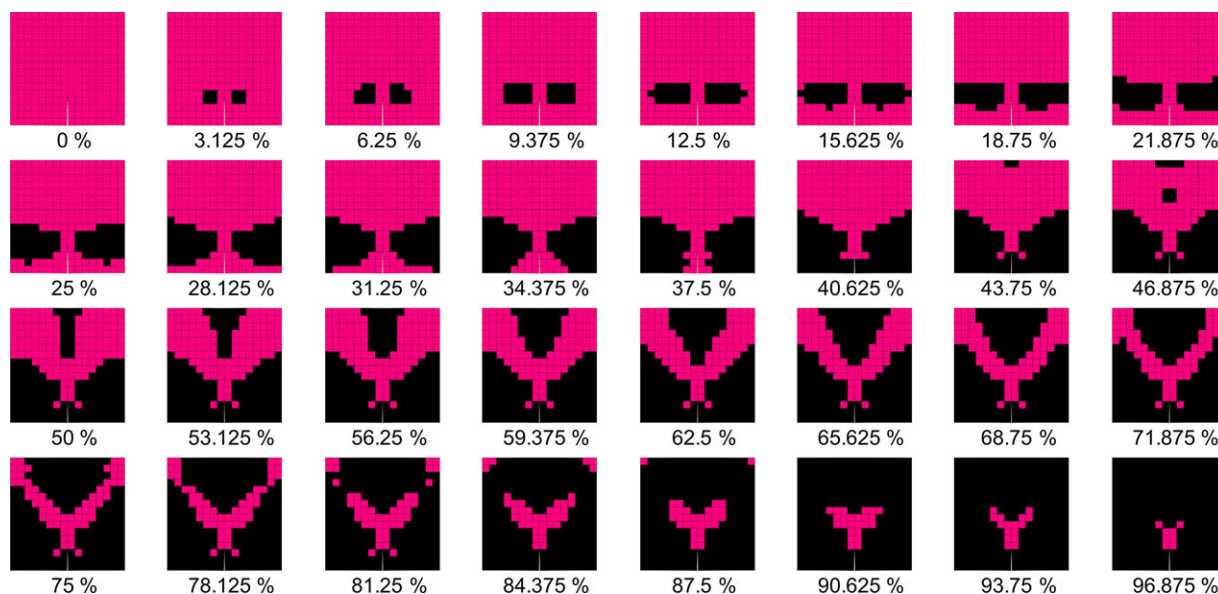


Figure 5. Optimal designs for high toughness, using base materials with the modulus ratio of 2 and toughness ratio of 2, for the 16 by 16 composite system. The results are obtained by machine learning for different volume fractions. The stiff elements are shown in pink and the soft elements are shown in black. The number below each optimal design is the volume fraction of the design.

algorithm to search for high-performing designs of hierarchical composites. On the other hand, the linear model and nonlinear model can generate optimal designs directly after the training process, without the need for any searching (see the Experimental Section for details). Moreover, among these two ML models, the nonlinear model performs much better than the linear model, especially on the highly ranked samples. Thus, to balance the accuracy and efficiency, the nonlinear model is adopted to generate optimal designs for larger composite systems. The computational cost of the ML approach compared to the finite element analysis is discussed in the Supporting Information. In general, the ML approach provides more than a 100 000-fold speedup.

Here, we consider a 16 by 16 composite system with the modulus ratio of 2 and toughness ratio of 2 to simulate graphene and graphane. The system has a design space of 2^{128} combinations as geometrical symmetry is assumed. Equipped with a highly accurate and efficient ML model, searching for the optimal designs of larger composite systems is now possible. After the training process, the optimal designs for different volume fractions generated by the ML model (nonlinear model) are shown in **Figure 5**. It can be observed that the design strategy to achieve high toughness is different from that observed in **Figure 1**; **Figures S8 and S9**, Supporting Information in which the toughness of the base materials is the same. In **Figure 1**; **Figures S8 and S9**, Supporting Information, as mentioned before, a common design strategy to achieve high toughness is to use the soft material for the crack-tip elements and the stiff material for the elements above and below the crack-tip elements. However, as shown in **Figure 5**, using the soft material for the crack-tip elements is no longer a good idea. In fact, the optimal design shown in **Figure 5** have no soft material at the crack tip. The reason is that the soft material used in **Figure 1**; **Figures S8 and S9**, Supporting Information. In the composite system shown in **Figure 5**, the stiff and soft materials

have the same failure strain ($\epsilon_{f, \text{soft}}/\epsilon_{f, \text{stiff}} = 1$) as the modulus and toughness ratios are the same. Thus, using the soft material for the crack-tip elements cannot aid in the postponement of crack propagation. In fact, it is not ideal since the soft material has only 50% of the toughness of the stiff material.

To evaluate the performance of the optimal designs generated by the ML model, we first consider an 8 by 8 composite system with a modulus ratio of 2 and toughness ratio of 2. We compare the toughness of the ML designs for different volume fractions with the optimal designs identified by the brute-force search. **Figure 6a** shows that the toughness of the ML designs is almost identical to that of the optimal designs identified by the brute-force search. We want to make a note that the ML solutions are not necessarily global minima (the best designs) in any formal sense; our goal is to find solutions that are not poor local minima and close enough to global minima. More discussions on the issue of local minima in the composite design problems can be found in the Supporting Information. Note that the toughness of the ML designs for the volume fraction lower than 21.875% or higher than 78.125% is not shown in **Figure 6a** because the number of possible combinations in an 8 by 8 composite system with the volume fraction in these ranges is less than the number of samples (1 000 000) required for training and testing the ML model. With the success in the 8 by 8 composite system, we consider a 16 by 16 composite system with the modulus ratio of 2 and toughness ratio of 2, in which the ML designs are shown in **Figure 5**. Although we cannot generate brute-force search results for comparison due to computational limitations, it can be observed that the toughness of the ML designs is much higher than that of the training samples (**Figure 6b**). Additionally, **Figure 6b** shows that the optimal volume fraction for high toughness is 40.625% for the composite system considered here. The property distributions of the training samples with this volume fraction (40.625%) are shown in **Figure 6c,d**. It can be observed that the

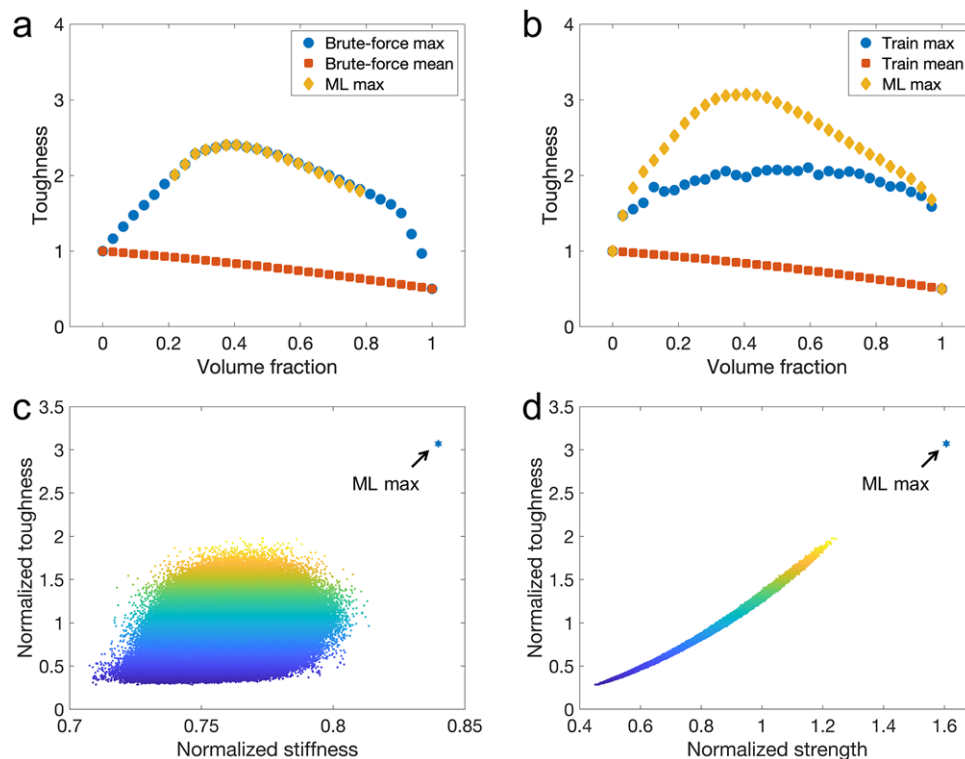


Figure 6. Performance of the optimal designs generated by machine learning compared to the brute-force search results for the 8 by 8 composite system. b) shows the toughness of the optimal designs generated by machine learning compared to the highest toughness and mean toughness of the training samples for the 16 by 16 composite system. The optimal volume fraction for high toughness is found as 40.625%. c) shows the toughness and stiffness of the optimal design generated by machine learning compared to the training samples for the 16 by 16 system with the optimal volume fraction. d) shows the toughness and strength of the optimal design generated by machine learning compared to the training samples for the 16 by 16 system with the optimal volume fraction. In these composite systems, the modulus and toughness ratios are set to 2. The color in (c) and (d) represents the toughness values of the training samples.

correlation between stiffness and toughness is weak (Figure 6c). On the other hand, the correlation between strength and toughness is strong (Figure 6d), which suggests that if a composite design has high strength, it also has high toughness, and vice versa. Compared with the training samples, the ML design has much higher toughness, which is expected as the ML model is trained to generate designs for high toughness. Although the ML model is not trained to generate designs for high strength, the ML design also has much higher strength. The reason is that the strength value and toughness value are highly correlated. Interestingly, the stiffness of the ML design is also much higher than that of the training samples. These results show that the ML model can learn the structure–property relationships from training data and generate designs with much better performance.

2.4. Graphene Nanocomposite Design from Machine Learning

To study whether the toughening and strengthening mechanism due to the geometrical effect of combining stiff and softer material is valid for nanomaterials, a graphene nanocomposite made up of graphene (stiff) and graphane (soft) with the topology designed by machine learning is investigated. The optimal design with the optimal volume fraction (40.625%) is adopted from Figure 5 to create an MD model for the graphene nanocompos-

ite. MD models for graphene and graphane are also created for comparison. As with the FEM models, these MD models have an edge crack of 25% of the model width in the y -direction, and displacement boundary conditions are applied along the x -direction to simulate *Mode I* fracture. The details of these MD models are shown in Figure 7a. Before running tensile tests to simulate *Mode I* fracture, these MD models are fully relaxed to eliminate the initial stresses (see the Experimental Section for details). Figure 7b shows the force–strain curves of the graphene, graphane, and graphene nanocomposite models, under *Mode I* fracture. From the force–strain curves, the modulus ratio of graphene and graphane can be approximated to 2 and the toughness ratio can be approximated to 2, as well. These are the modulus and toughness ratios adopted in the ML model to generate the optimal design in the previous section. Note that the exact modulus ratio cannot be defined since the force–strain curves are not completely linear. In Figure 7b, it can be observed that the graphene nanocomposite model (designed by machine learning) has higher toughness and strength compared to its base materials. Additionally, the ML predictions (Figure 6b) based on the FEM results (continuum-scale analysis) show that the optimal design has toughness of about 310% of the toughness of the stiff material (i.e., graphene). In the MD simulations (Figure 7b), the toughness of the graphene nanocomposite model is about 210% of the toughness of the graphene model. The toughness

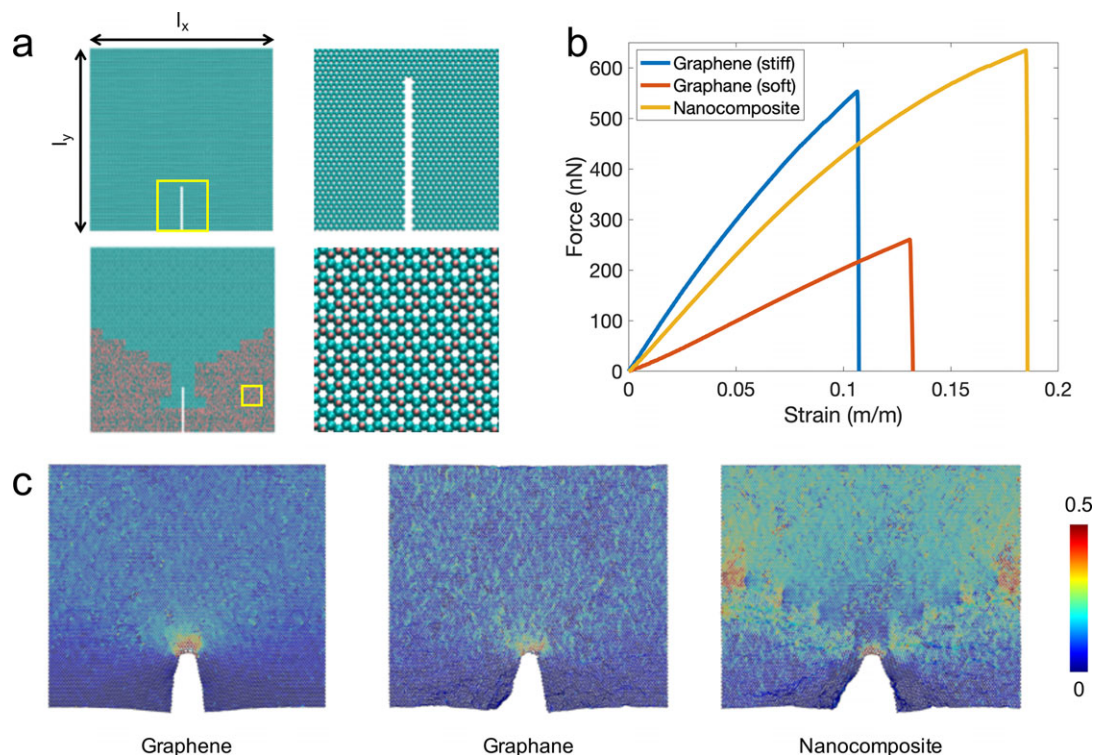


Figure 7. Performance of the graphene nanocomposite designed by machine learning. a) The atomistic models of pure graphene and graphene nanocomposite. Zoomed-in images from the yellow-boxed regions are shown on the right. Green represents carbon atoms and pink represents hydrogen atoms. b) shows the force–strain curves of the graphene, graphane, and graphene nanocomposite models under the tensile tests. In this composite system, graphene and graphane are adopted as the base materials, in which graphene serves as the stiff material and graphane serves as the soft material. c) shows the strain fields of the graphene, graphane, and graphene nanocomposite models before crack propagation. The color in (c) represents the strain values.

improvement observed in the MD simulations is on the same order of magnitude as the ML predictions. Therefore, we confirm the hypothesis that the toughening and strengthening mechanism due to the geometrical effect of combining stiff and soft material is valid for both continuum-scale and nanoscale composites.

Figure 7c shows the strain fields (ϵ_{xx}) of the graphene, graphane, and graphene nanocomposite models at the critical loading condition (close to the point of crack propagation). It can be observed that there is a significant strain concentration at the crack tip in the strain fields of the graphene and graphane models, whereas the strains at other regions remain very low. This is the typical behavior of a homogeneous material under *Mode I* fracture. In the strain field of the graphene nanocomposite model, although there is also a strain concentration at the crack tip, the strains at other regions are also very high. This uniform strain distribution is due to the fact that the geometrical effect of combining stiff and soft material delocalizes the strain concentration at the crack tip. Consequently, compared with its base materials, more elastic energy can be stored in the graphene nanocomposite model prior to failure. Comparison of strain fields before and after crack propagation is shown in Figure S13, Supporting Information. Note that the dimension of the graphene nanocomposite model is 280 Å by 280 Å and the design grid is 16 by 16. Thus, the design resolution is 17.5 Å. It is currently very challenging to fabricate the design with such

high resolution. However, in recent years, the fabrication techniques for hydrogenated graphene and other 2D materials have been significantly improved. A promising recent study showed that nanoresolution patterning on hydrogenated graphene can be realized with the resolution of the patterning up to 18 nm.^[12]

3. Conclusions

In this work, we present a systematic computational investigation on the effect of constituent materials on the behavior of composites under *Mode I* fracture. By using the brute-force search, we show that composites made out of stiff and soft materials with random designs, statistically, are tougher than the base materials alone. Moreover, for those composites with optimal designs, depending on the properties of the base materials, the effective toughness can be orders of magnitude higher than the base materials alone. We show that a higher toughness improvement can be expected when the modulus ratio of base materials is higher. That is to say, when choosing a soft material to pair with a stiff material, a soft material with a lower modulus will give rise to a higher toughness improvement. In addition to the modulus ratio, the toughness ratio of base materials is also critical. Results show that the toughness improvement decreases as the toughness ratio of base materials increases. In other words, a high toughness improvement can be expected only when the toughness of the

soft material is comparable to that of the stiff material. The effect of base materials on the strength of composites is similar to that on the toughness. Therefore, an ideal soft material to pair with a stiff material for high toughness and strength improvements is a soft material with low modulus and high toughness at the same time. We demonstrate that, instead of using computationally expensive brute-force methods to search for the optimal designs of composites, using machine learning is a much more efficient approach. We show that, with a proper hypothesis, highly accurate ML predictions can be achieved and the optimal designs of composites can be generated directly without requiring any sampling, screening, or optimization process. Results show that our ML-based approach can generate high-performing designs comparable to the brute-force search results and only costs a fraction of the computational time. Consequently, our ML-based approach can be applied to designing larger composite systems, in which using brute-force methods is computationally prohibitive. Finally, we use graphene and graphane as base materials to create a graphene nanocomposite with the topology designed by machine learning. As demonstrated in our MD simulations, our graphene nanocomposite has higher toughness and strength compared to its base materials. The result complements our finite element analysis and confirms that the toughening and strengthening mechanism due to the geometrical effect of combining stiff and soft materials is also valid for nanomaterials.

4. Experimental Section

Finite Element Analysis: The composite design domain is discretized by square elements. Four-node elements are implemented with an assumption that the failure of elements occurs in the linear elastic regime. The stiffness matrix of the four-node elements is shown in the Supporting Information. An edge crack of 25% of the specimen width in the y -direction is created by the insertion of double nodes. Displacement boundary conditions are applied along the x -direction to simulate *Mode I* fracture. Geometrical symmetry is assumed in the composites since the edge crack is located at the centerline of the specimen and the loading condition is symmetric. The modulus of the stiff material is set to 1 GPa and the Poisson ratio is set to 1/3. The failure strain of the stiff material is set to 10%, regardless of what modulus and toughness ratios are adopted in a composite system. On the other hand, the failure strain of the soft material is determined based on the modulus and toughness ratios in a composite system. Note that the modulus of 1 GPa and the failure strain of 10% for the stiff material can be changed to any other positive values without altering the results shown in this work. The optimal designs of composites only depend on the relative properties (e.g., the modulus and toughness ratios) of the base materials. After applying displacement boundary conditions, the strain in the loading direction (ϵ_{xx}) at the crack tip is used to calculate the toughness and strength of a composite. Once the strain reaches the failure strain of crack-tip elements (stiff and soft materials typically have different failure strains), the composite is considered to have failed and its toughness (area underneath the stress–strain curve) and strength (maximum stress) can be determined. The resistance of composites during crack propagation is not considered here; instead, due to computational limitations, the resistance of composites to initiate crack propagation was considered.

Machine Learning Approach: ML calculations are performed using TensorFlow, an open-source software library for machine learning applications.^[13] The geometries of training and testing samples are randomly generated with the geometrical symmetry constraint. Their quantitative metrics (i.e., toughness, strength, and stiffness) are calculated using finite element analysis. Three ML models are investigated in this work:

linear, nonlinear, and CNN models. The first ML model considered is a linear model. The hypothesis in this model is:

$$y = \mathbf{w}^T \mathbf{x} + b \quad (2)$$

where \mathbf{w} and b are weights and bias, respectively. \mathbf{x} represents input data (the geometry of a composite) and y represents the prediction (the scaled toughness, strength, or stiffness). The second ML model considered is a nonlinear model. The hypothesis in this model is:

$$y = e^{\mathbf{w}^T \mathbf{x} + c} + \mathbf{w}^T \mathbf{x} + b \quad (3)$$

where \mathbf{w} and b are weights and bias, respectively. The new parameter c represents the weight ratio of the nonlinear contribution ($e^{\mathbf{w}^T \mathbf{x}}$) and linear contribution ($\mathbf{w}^T \mathbf{x}$). The values of \mathbf{w} , b , and c are optimized in the training process. A larger c means that the nonlinear contribution is more significant than the linear contribution. Using different hypotheses, other nonlinear models can be created. The hypothesis that was used in this nonlinear model is carefully selected as it is a monotonically increasing function with respect to $\mathbf{w}^T \mathbf{x}$. Thus, the following statement is valid:

$$\mathbf{w}^T \mathbf{x}_1 \geq \mathbf{w}^T \mathbf{x}_2 \rightarrow y(\mathbf{w}^T \mathbf{x}_1) \geq y(\mathbf{w}^T \mathbf{x}_2) \quad (4)$$

Therefore, the input data \mathbf{x}_i that gives the highest value of y is the same as the input data \mathbf{x}_j that achieves the highest value of $\mathbf{w}^T \mathbf{x}$. As the weights \mathbf{w} are known after the training process, the input data \mathbf{x} that gives the highest value of $\mathbf{w}^T \mathbf{x}$ (also the highest value of y) can be determined directly. Consequently, this nonlinear model can generate the optimal designs of composite systems directly without requiring any sampling, screening, or optimization process. The third ML model considered is a CNN model consisting of three hidden layers. The first two are convolutional layers with 32 features in the first layer and 64 features in the second layer. A patch of 3 by 3 and a stride of one with zero padding is adopted. The weights are initialized with some randomness, added with a small bias, and passed through the rectified linear unit (ReLU) activation function. The last layer is a fully connected layer with 256 neurons. Note that searching for the optimal hyperparameters for the CNN model is not a focus in this work.

The MSE is used to estimate the loss of these three ML models during the training and testing processes. The MSE is computed as:

$$\text{MSE} = \frac{1}{n} \sum_{i=1}^n (y_i - \hat{y}_i)^2 \quad (5)$$

where n is the number of samples used to calculate the MSE, y_i represents the prediction of sample i (from ML models) and \hat{y}_i represents the actual quantity of the sample (from finite element analysis). The training process for these three ML models is identical. 800 000 samples are used to train these ML models and 200 000 samples are used to evaluate their accuracy. Note that the training and testing samples are randomly generated. The training batch size is 10 000 and the training loop is 100 000.

Molecular Dynamics Modeling: Full-atomistic models for graphene, graphane, and the graphene nanocomposite are created for MD simulations. The dimension of these models is 280 Å by 280 Å in the x – y plane, and an edge crack of 25% of the model width (70 Å) in the y -direction is introduced to simulate *Mode I* fracture (Figure 7a). Graphane is a form of hydrogenated graphene with a formula CH. Hydrogen atoms are randomly added on either side of the graphene basal plane in the graphane model. Graphene and graphane are chosen as base materials to make a graphene nanocomposite, in which graphene serves as the stiff material and graphane serves as the soft material. MD simulations are implemented using Large-scale Atomic/Molecular Massively Parallel Simulator (LAMMPS).^[14] The adaptive intermolecular REBO potential (AIREBO)^[15] is implemented and the C–C bond cut-off distance is set to 1.95 Å.^[16] The time step is set to 0.25 fs to ensure the stability and to reflect the high vibration frequency of hydrogen atoms. The simulation box size in the x -direction is the same as the model length (280 Å) to keep

the periodicity in the x -direction (loading direction). However, to simulate *Mode I* fracture, the models should not be periodic in the y -direction. Thus, the periodicity in the y -direction is eliminated by adding a vacant space with a length of 20 Å. The simulation box size in the z -direction (out-of-plane direction) is set to 20 Å to ensure that the models do not interact with their periodic images in the z -direction.

Periodic boundary conditions (PBCs) are applied. The left and right edges (one-atom width) of the models are fixed in the z -direction and are free to move in the other two directions. Three steps of MD equilibrations are performed to fully relax the models. After energy minimization using the conjugate gradient (CG) algorithm, the systems are equilibrated with the canonical (NVT) ensemble at a constant temperature of 300 K for 10 ps. As the models are periodic in the x -direction, to ensure that the models are fully relaxed in the x -direction, the systems are then equilibrated with the isothermal–isobaric (NPT) ensemble at a constant temperature of 300 K and zero pressure in the x -direction for 10 ps. Finally, the systems are equilibrated again with the NVT ensemble at a constant temperature of 300 K for 10 ps. The pressures (x -, y -, and z -directions) of the systems during the MD equilibrations are shown in Figures S14–S16, Supporting Information. It can be seen that the pressures are converged to zero, showing that the systems are fully relaxed. Tensile tests using a displacement controlled method^[17] are performed to measure mechanical responses of the models under *Mode I* fracture. During the tensile tests, the simulation boxes are stretched in the x -direction with a constant engineering strain of 0.0001 applied every 1 ps, which is equivalent to an engineering strain rate of 0.1 ns^{-1} . For the size of the models, this strain rate is slow enough to accurately simulate mechanical responses of graphene in MD simulations.^[18] During the tensile tests, the systems are equilibrated with the NVT ensemble at a constant temperature of 300 K. Note that the graphene nanocomposite is made out of base materials with different thicknesses. The thickness of the graphene nanocomposite cannot be defined. Thus, instead of measuring the tensile stress in the models during the tensile tests, the tensile force was measured. Specifically, the tensile force in the loading direction (Figure 7b) is derived from the carbon atoms on the graphene basal plane excluding those on the left and right edges. The Open Visualization Tool (OVITO)^[19] and Visual Molecular Dynamics (VMD)^[20] are implemented for the visualization and strain analysis.

Supporting Information

Supporting Information is available from the Wiley Online Library or from the author.

Acknowledgements

The authors acknowledge support from the Regents of the University of California, Berkeley. This work used the Extreme Science and Engineering Discovery Environment (XSEDE) Bridges system at the Pittsburgh Supercomputing Center (PSC) through allocation TG-DMR180085, which was supported by National Science Foundation grant number ACI-1548562. Additionally, the authors acknowledge support from the Savio computational cluster resource provided by the Berkeley Research Computing program.

Conflict of interest

The authors declare no conflict of interest.

Keywords

composites, finite elements, graphene, machine learning, molecular dynamics

Received: March 16, 2019

Published online:

- [1] a) B. G. Compton, J. A. Lewis, *Adv. Mater.* **2014**, *26*, 5930; b) A. R. Stuard, *Adv. Funct. Mater.* **2013**, *23*, 4423; c) Y. Sun, N. Pugno, *Materials* **2013**, *6*, 699; d) J. Wang, Q. Cheng, Z. Tang, *Chem. Soc. Rev.* **2012**, *41*, 1111; e) J. Yeo, G. S. Jung, F. J. Martín-Martínez, S. Ling, G. X. Gu, Z. Qin, M. J. Buehler, *Phys. Scr.* **2018**, *93*, 053003.
- [2] a) N. Iyengar, W. Curtin, *Acta Mater.* **1997**, *45*, 3419; b) G. X. Gu, M. Takaffoli, A. J. Hsieh, M. J. Buehler, *Extreme Mech. Lett.* **2016**, *9*, 317; c) G. X. Gu, L. Dimas, Z. Qin, M. J. Buehler, *J. Appl. Mech.* **2016**, *83*, 071006; d) T. Verho, P. Karppinen, A. H. Gröschel, O. Ikkala, *Adv. Sci.* **2018**, *5*, 1700635.
- [3] a) S. Das, D. L. Bourell, S. Babu, *MRS Bull.* **2016**, *41*, 729; b) I. Gibson, D. Rosen, B. Stucker, *Additive Manufacturing Technologies: 3D Printing, Rapid Prototyping, and Direct Digital Manufacturing*, Springer, New York **2014**; c) S. A. Goehrke, *Metal 3D Printing with Machine Learning: GE Tells Us About Smarter Additive Manufacturing*, 3Dprint.com. **2017**.
- [4] a) N. Guo, M. C. Leu, *Front. Mech. Eng.* **2013**, *8*, 215; b) Y. Huang, M. C. Leu, J. Mazumder, A. Donmez, *J. Manuf. Sci. Eng.* **2015**, *137*, 014001; c) F. P. Melchels, M. A. Domingos, T. J. Klein, J. Malda, P. J. Bartolo, D. W. Huttmacher, *Prog. Polym. Sci.* **2012**, *37*, 1079; d) L. E. Murr, E. Martinez, K. N. Amato, S. M. Gaytan, J. Hernandez, D. A. Ramirez, P. W. Shindo, F. Medina, R. B. Wicker, *J. Mater. Res. Technol.* **2012**, *1*, 42; e) N. Raghavan, R. Dehoff, S. Pannala, S. Simunovic, M. Kirka, J. Turner, N. Carlson, S. S. Babu, *Acta Mater.* **2016**, *112*, 303.
- [5] C.-T. Chen, F. J. Martín-Martínez, S. Ling, Z. Qin, M. J. Buehler, *Nano Futures* **2017**, *1*, 011003.
- [6] a) G. X. Gu, F. Libonati, S. D. Wettermark, M. J. Buehler, *J. Mech. Behav. Biomed. Mater.* **2017**, *76*, 135; b) G. X. Gu, M. Takaffoli, M. J. Buehler, *Adv. Mater.* **2017**, *29*, 1700060; c) F. Libonati, G. X. Gu, Z. Qin, L. Vergani, M. J. Buehler, *Adv. Eng. Mater.* **2016**, *18*, 1354; d) P.-Y. Chen, J. McKittrick, M. A. Meyers, *Prog. Mater. Sci.* **2012**, *57*, 1492; e) J. W. Dunlop, R. Weinkamer, P. Fratzl, *Mater. Today* **2011**, *14*, 70; f) G. X. Gu, I. Su, S. Sharma, J. L. Voros, Z. Qin, M. J. Buehler, *J. Biomech. Eng.* **2016**, *138*, 021006; g) J. Mueller, J. R. Raney, D. M. Kochmann, K. Shea, *Adv. Sci.* **2018**, *5*, 1800728.
- [7] a) M. P. Bendsøe, O. Sigmund, *Topology Optimization by Distribution of Isotropic Material*, Springer, Berlin **2004**; b) D. Brackett, I. Ashcroft, R. Hague, presented at Proc. of the Solid Freeform Fabrication Symposium, Austin, TX, August 2011; c) H. A. Eschenauer, N. Olhoff, *Appl. Mech. Rev.* **2001**, *54*, 331; d) A. T. Gaynor, N. A. Meisel, C. B. Williams, J. K. Guest, *J. Manuf. Sci. Eng.* **2014**, *136*, 061015; e) T. Ziegler, G. H. Paulino, *Struct. Multidiscip. Optim.* **2016**, *53*, 175; f) G. X. Gu, M. J. Buehler, *Acta Mech.* **2018**, *229*, 4033.
- [8] a) R. Liu, A. Kumar, Z. Chen, A. Agrawal, V. Sundararaghavan, A. Choudhary, *Sci. Rep.* **2015**, *5*; b) R. S. Michalski, J. G. Carbonell, T. M. Mitchell, *Machine Learning: An Artificial Intelligence Approach*, Springer Science+Business Media, Berlin **2013**; c) G. P. P. Wang, X. Jiang, S. Rajasekaran, R. Ramprasad, *Sci. Rep.* **2013**, *3*; d) N. K. Hansoge, T. Huang, R. Sinko, W. Xia, W. Chen, S. Ketan, *ACS Nano* **2018**, *12*, 7946; e) A. Mannodi-Kanakkithodi, A. Chandrasekaran, C. Kim, T. D. Huan, G. P. P. Wang, V. Botu, R. Ramprasad, *Mater. Today* **2018**, *21*, 785.
- [9] G. X. Gu, C.-T. Chen, M. J. Buehler, *Extreme Mech. Lett.* **2018**, *18*, 19.
- [10] G. X. Gu, C.-T. Chen, D. J. Richmond, M. J. Buehler, *Mater. Horiz.* **2018**, *5*, 939.
- [11] P. Z. Hanakata, E. D. Cubuk, D. K. Campbell, H. S. Park, *Phys. Rev. Lett.* **2018**, *121*, 255304.
- [12] J. Liu, S. Chen, R. Papadakis, H. Li, *Nanotechnol.* **2018**, *29*, 415304.
- [13] M. Abadi, P. Barham, J. Chen, Z. Chen, A. Davis, J. Dean, M. Devin, S. Ghemawat, G. Irving, M. Isard, presented at Proc. of the 12th

- USENIX Symp. on Operating Systems Design and Implementation (OSDI'16), Savannah, GA, November 2016.
- [14] S. Plimpton, *J. Comput. Phys.* **1995**, 117, 1.
- [15] S. J. Stuart, A. B. Tutein, J. A. Harrison, *J. Chem. Phys.* **2000**, 112, 6472.
- [16] a) L. He, S. Guo, J. Lei, Z. Sha, Z. Liu, *Carbon* **2014**, 75, 124; b) Y. Zhang, C. Wang, Y. Cheng, Y. Xiang, *Carbon* **2011**, 49, 4511.
- [17] C.-T. Chen, S. Ghosh, C. M. Reddy, M. J. Buehler, *Phys. Chem. Chem. Phys.* **2014**, 16, 13165.
- [18] G. Jung, Z. Qin, M. J. Buehler, *Extreme Mech. Lett.* **2015**, 2, 52.
- [19] A. Stukowski, *Modell. Simul. Mater. Sci. Eng.* **2009**, 18, 015012.
- [20] W. Humphrey, A. Dalke, K. Schulten, *J. Mol. Graphics* **1996**, 14, 33.